EPiC Series in Computing

Volume 104, 2024, Pages 1–13

Proceedings of 3rd International Workshop on
Mathematical Modeling and Scientific Computing

Trade-Offs in Robust Trajectory Optimization Based on Sensitivity Minimization*

Tuğba Akman and Florian Holzapfel

Institute of Flight System Dynamics, Technical University of Munich,
Garching, Germany
{tugba.akman, florian.holzapfel}@tum.de

Abstract

Rapid developments in aerospace technologies demand reliable procedures to plan robust missions with high safety. To increase safety under uncertainties in model parameters or environmental conditions, multi-objective robust optimization methods via sensitivity minimization can be used. An acceptable trade-off between a nominal operational cost (e.g., time, energy) and robustness is searched for to plan missions that are less prone to disturbances. The presented analysis considers open-loop and closed-loop sensitivity minimization approaches and utilizes multi-objective optimization to assess the performance and the limitations of both approaches. To solve the multi-objective optimization problems, scalarization techniques are employed using weighted sums and cost bounds. By varying weights and cost bounds, multiple optima can be calculated, resulting in an approximate Pareto front and giving rise to an overview of the trade-off between optimality and robustness of the solutions. The analysis is performed for robust unmanned aerial vehicle (UAV) trajectory optimization minimizing positional sensitivities.

1 Introduction

When planning missions in aerospace engineering, robustness is essential to increase safety and reduce costs, especially for various unmanned aerial vehicle (UAV) applications. Robustness is crucial, e.g., when designing trajectories to achieve high performance under uncertain circumstances. In [13], trajectory optimization for UAV take-off regarding positional robustness is studied using stochastic collocation. In [18], sensitivity minimization is employed to increase the robustness of battery pack temperatures.

However, when increasing robustness, there is a trade-off between multiple important factors, e.g., resources, costs, and safety. In order to find the best compromise between optimality and robustness with the given resources, multi-objective optimization can be applied. Multiple costs, mostly conflicting, are minimized simultaneously to meet user-specified requirements. Often, there are multiple compromises, which a Pareto front can represent. Points on the Pareto front

*This research was funded by the German Federal Ministry for Economic Affairs and Climate Action through the project OPTIMISTIC (grant number 20Q1936B).

are solutions of a multi-objective optimization problem, such that no single cost function value can be improved without deteriorating another. There are different approaches for calculating Pareto optimal solutions. An overview of solution approaches is given in [12, 11]. Further theoretical details referring to, e.g., non-convexity, are presented in [7]. Classically, a posteriori methods aim to generate multiple Pareto optimal points from which a decision maker can select the most suitable compromise. Most of these multi-objective approaches aim to formulate a problem with a scalar cost function. The main challenge is a proper formulation of the problem in order to generate a representative set of Pareto optimal solutions and to ensure a proper basis for selecting an appropriate solution. Here, computational resources, completeness, and accuracy of the Pareto front are of main interest.

Related studies in the field of multi-objective UAV trajectory optimization are presented in [15], where two objectives, namely flight time and risk to the human population, are minimized. The authors from [17] analyze the trade-off between transmission time and energy consumption for UAV communication networks with multi-objective particle swarm optimization. In [1], the authors have investigated a trade-off in the robustness of UAV climb trajectories using open-loop and closed-loop considerations. The paper at hand is based on the work in [1] and extends it by a holistic robustness analysis, systematically calculating multiple trade-offs for UAV trajectory optimization using optimal control to further assess the performance and limitations of the open-loop and closed-loop modeling approaches. For this, three objectives, a nominal operational cost and two positional sensitivity costs, are minimized using different scalarization methods for multi-objective optimization.

This study is structured as follows. First, the multi-objective robust optimal control problems in open-loop and closed-loop are stated in Section 2. Afterward, the utilized scalarization techniques are presented in Section 3. A description of the application scenario for UAV trajectory optimization is stated in Section 4, followed by numerical results and their discussion. The analysis is concluded in Section 5.

2 Multi-objective optimal control problem statements

This section presents a general optimal control problem formulation with multiple cost functions, namely a nominal operational cost and sensitivity costs for robustness based on [10, 5, 1]. To analyze open-loop and closed-loop modeling approaches with respect to robustness, both modeling approaches are included in the optimal control problem formulation in the following subsections according to [1].

2.1 Open-loop optimal control problem statement minimizing operational cost and sensitivity

Usually, an open-loop model is the first basis for trajectory optimization, as it builds a crucial base in developing a flight system. An open-loop multi-objective robust optimal control problem minimizing sensitivities regarding uncertainties can be formulated as follows. The aim is to find a state history $\mathbf{x}\colon \mathcal{T} \to \mathbb{R}^{n_x}$ and a control history $\mathbf{u}\colon \mathcal{T} \to \mathbb{R}^{n_u}$, where the considered time horizon is denoted by $\mathcal{T} = [t_0, t_f] \subseteq \mathbb{R}$, which solve the following problem:

$$\min_{\mathbf{x},\mathbf{u},t_f} \begin{bmatrix} J_0 & J_{S_1} & \dots & J_{S_{n_J}} \end{bmatrix} \tag{1}$$

with a nominal operational cost

$$J_0 = J(\mathbf{x}(t_0), \mathbf{x}(t_f), t_f) \tag{2}$$

and sensitivity costs

$$J_{S_i} = \int_{t_0}^{t_f} S_i(t)^2 \, dt, \quad i = 1, \ldots, n_J \tag{3}$$

to increase robustness, subject to the dynamic constraints

$$\dot{\mathbf{x}}(t) = \mathbf{f}(\mathbf{x}(t), \mathbf{u}(t); \mathbf{p}) \tag{4}$$

with $\mathbf{f}\colon \mathbb{R}^{n_x} \times \mathbb{R}^{n_u} \to \mathbb{R}^{n_x}$, the sensitivity differential equation according to [5] for sensitivities $\mathbf{S}\colon \mathcal{T} \to \mathbb{R}^{n_x} \times \mathbb{R}^{n_p}$ with $\mathbf{S}(t) \coloneqq \frac{\partial \mathbf{x}}{\partial \mathbf{p}}(t)$ and

$$\dot{\mathbf{S}}(t) = \frac{\partial \mathbf{f}}{\partial \mathbf{x}}(t) \cdot \mathbf{S}(t) + \frac{\partial \mathbf{f}}{\partial \mathbf{p}}(t), \quad \mathbf{S}(t_0) = \frac{\partial \mathbf{x}}{\partial \mathbf{p}}(t_0), \tag{5}$$

the initial and final boundary conditions

$$\boldsymbol{\psi}(\mathbf{x}(t_0), \mathbf{x}(t_f); \mathbf{p}) = \mathbf{0} \tag{6}$$

with $\boldsymbol{\psi}\colon \mathbb{R}^{n_x} \times \mathbb{R}^{n_x} \to \mathbb{R}^{n_\psi}$, linear inequality constraints

$$\mathbf{c}_{ineq}(\mathbf{x}(t), \mathbf{u}(t); \mathbf{p}) \leq \mathbf{0} \tag{7}$$

and linear rate constraints

$$\mathbf{c}_{rate}(\dot{\mathbf{x}}(t), \dot{\mathbf{u}}(t); \mathbf{p}) \leq \mathbf{0} \tag{8}$$

for all $t \in \mathcal{T}$ with $\mathbf{c}_{ineq}\colon \mathbb{R}^{n_x} \times \mathbb{R}^{n_u} \to \mathbb{R}^{n_{ineq}}$ and $\mathbf{c}_{rate}\colon \mathbb{R}^{n_x} \times \mathbb{R}^{n_u} \to \mathbb{R}^{n_{rate}}$. The parameter $\mathbf{p} \in \mathbb{R}$ represents the model uncertainty and is fixed to a nominal value $\mathbf{p}_0$. The problem formulation can be extended to consider multiple uncertainties. Since, in this study, a scalar uncertain parameter is considered, the notation is restricted to the scalar case.

The cost function J_0 is a Mayer cost function, representing operational costs, e.g., energy consumption or flight time. The cost functions J_{S_i} with $i \geq 1$ are integrated squared sensitivities, describing the states' dependencies on model parameters. For notational ease in the cost function, the sensitivities are numbered, e.g., S_i may describe the sensitivity of the i-th state. Minimizing sensitivities is of interest when designing robust trajectories. A reduced sensitivity increases robustness against parameter perturbations. Usually, the operational and sensitivity costs are conflicting, i.e., when one cost function is decreased, at least another increases. In other words, there is a trade-off between optimality and robustness. Therefore, multi-objective optimization is suitable for selecting trajectory designs with an acceptable trade-off between operational costs and robustness.

2.2 Closed-loop optimal control problem statement minimizing operational cost and sensitivity

Since, in reality, the system operates in closed-loop, its robustness is increased. Nevertheless, it is desired to exploit the full system performance, and hence, it is meaningful to further reduce sensitivities. Therefore, the multi-objective robust optimal control problem in Section 2.1 is extended to a closed-loop formulation. The following closed-loop formulation is adapted from the work [1].

Let $\mathbf{p}$ be a realization of the uncertainty. It is assumed that the realizations are in a bounded set $\mathbf{P} \subset \mathbb{R}$ with $\mathbf{p}_{lb} \leq \mathbf{p} \leq \mathbf{p}_{ub}$ for $\mathbf{p}_{lb}, \mathbf{p}_{ub} \in \mathbf{P}$. A feasible control for the open-loop problem

(1) – (8) is denoted by $\mathbf{u}(\cdot;\mathbf{p}_0)\colon \mathcal{T} \to \mathbb{R}^{n_u}$. Then, a control update $\hat{\mathbf{u}}\colon \mathcal{T} \times \mathbf{P} \to \mathbb{R}^{n_u}$ with a predicted feedback is defined by

$$\hat{\mathbf{u}}(t,\mathbf{p}) = \mathbf{u}(t;\mathbf{p}_0) + \mathbf{K}(t) \cdot \mathbf{S}(t) \cdot (\mathbf{p} - \mathbf{p}_0)\,. \tag{9}$$

It is to be noted that a parameter value is usually estimated, and its estimation can be used to update the control. The performance of the updated control depends on the estimation accuracy of a parameter realization.

Compared to the open-loop problem, the nominal controls $\mathbf{u}(\cdot;\mathbf{p}_0)$ are optimized together with the time-dependent gains $\mathbf{K}\colon \mathcal{T} \to \mathbb{R}^{n_u} \times \mathbb{R}^{n_x}$. In equation (9), these can be interpreted as the effect of state deviations on the control, i.e., $\mathbf{K}(t) \coloneqq \frac{\partial \hat{\mathbf{u}}(t,\mathbf{p})}{\partial \mathbf{x}}$. Then, the sensitivity differential equation (5) extends to

$$\dot{\mathbf{S}}(t) = \left(\frac{\partial \mathbf{f}}{\partial \mathbf{x}}(t) + \frac{\partial \mathbf{f}}{\partial \hat{\mathbf{u}}}(t) \cdot \mathbf{K}(t)\right) \cdot \mathbf{S}(t) + \frac{\partial \mathbf{f}}{\partial \mathbf{p}}(t), \quad \mathbf{S}(t_0) = \frac{\partial \mathbf{x}}{\partial \mathbf{p}}(t_0) \tag{10}$$

according to [16]. In comparison, for the open-loop case in equation (5) the term $\mathbf{K}(t) = \frac{\partial \mathbf{u}(t;\mathbf{p}_0)}{\partial \mathbf{x}}$ is zero, as the controls are subject to optimization and do not explicitly depend on $\mathbf{x}$.

As the gains are design variables, the path constraints (7) are extended by user-specified constraints for the gains:

$$\mathbf{K}_{lb} \leq \mathbf{K}(t) \leq \mathbf{K}_{ub} \tag{11}$$

for all $t \in \mathcal{T}$ with $\mathbf{K}_{lb}, \mathbf{K}_{ub} \in \mathbb{R}^{n_u \times n_x}$. Analogous to the optimal open-loop controls, the control updates are subject to path and rate constraints at the lower and upper bounds of $\mathbf{p}$ under the assumption that the worst-case deviations occur at these bounds:

$$\mathbf{c}_{ineq}(\mathbf{x}(t), \hat{\mathbf{u}}(t,\mathbf{p}_{lb});\mathbf{p}_{lb}) \leq \mathbf{0}, \quad \mathbf{c}_{ineq}(\mathbf{x}(t), \hat{\mathbf{u}}(t,\mathbf{p}_{ub});\mathbf{p}_{ub}) \leq \mathbf{0}, \tag{12}$$

$$\mathbf{c}_{rate}(\dot{\mathbf{x}}(t), \dot{\hat{\mathbf{u}}}(t,\mathbf{p}_{lb});\mathbf{p}_{lb}) \leq \mathbf{0}, \quad \mathbf{c}_{rate}(\dot{\mathbf{x}}(t), \dot{\hat{\mathbf{u}}}(t,\mathbf{p}_{ub});\mathbf{p}_{ub}) \leq \mathbf{0}. \tag{13}$$

3 Scalarization methods

Since common direct optimal control methods require a scalar cost function, the multi-objective problems from Section 2 are reformulated with a scalar cost function in the following subsections. The method selection is based on the overview given in [12]. Please note that for the subsequent problem statements, the constraints (4) – (8) and (10) – (13), respectively, are adopted. The modifications are made within the cost function and, if necessary, further constraints are imposed.

3.1 Weighted sum method

A common approach to tackle the sensitivity minimization problems in Section 2 is the weighted sum approach:

$$\min_{\mathbf{x},\mathbf{u},t_f} \; w_0 c_{s,0} J_0 + \sum_{i=1}^{n_J} w_i c_{s,i} J_{S_i}.$$

The weights w_i with $\sum_{i=0}^{n_J} w_i = 1$ can be specified by the decision maker. The higher the weight, the more the according cost is reduced. That means, if high optimality is required, the weight w_0 for the nominal cost is increased. If high robustness is required, the weights w_i for

$i \geq 1$ are increased. By varying the weights, a Pareto front can be generated if it is convex. However, not all Pareto optimal points can be calculated if the Pareto front is non-convex [12, 7]. Furthermore, an equidistant selection of weights does not ensure that equidistant Pareto optimal solutions are obtained, especially when the costs are in different orders of magnitude. If the weights are not modified accordingly, the solutions may accumulate close to the minimum cost value with a higher order of magnitude. Hence, a relevant region with actual trade-offs may be missed. The authors in [11, 3, 6, 9, 4] propose systematic selections of weights to ensure that the solutions map relevant regions with acceptable trade-offs. In this study, due to the different orders of magnitude between the final time cost and sensitivity cost in the open-loop case, each weighted cost term is scaled by a factor $c_{s,i}$ such that each term is in a similar order of magnitude to improve the balance between the cost terms.

Due to the convenience of implementation, the weighted sum approach is often used in robust optimization using sensitivity penalty, enabling the prioritization of minimizing nominal operational costs.

3.2 ε-constraint method

In the ε-constraint method, one cost function is minimized while constraining the other costs as follows:

$$\begin{aligned} &\min_{\mathbf{x},\mathbf{u},t_f} J_0 \\ &\text{s.t.} \quad J_{S_i} \leq \varepsilon_{i,0}, \quad i = 1, \ldots, n_J \end{aligned}$$

and vice versa

$$\begin{aligned} &\min_{\mathbf{x},\mathbf{u},t_f} J_{S_j} \\ &\text{s.t.} \quad J_0 \leq \varepsilon_{0,j} \\ &\qquad J_{S_i} \leq \varepsilon_{i,j}, \quad i = 1, \ldots, n_J, \quad i \neq j \end{aligned}$$

for all $j = 1, \ldots, n_J$. Thereby, the upper bound $\varepsilon_{i,j}$ can be defined to be in a range of the minimum of J_{S_i} and the value that J_{S_i} takes when the cost J_{S_j} is minimized, i.e., $\varepsilon_{i,j} \in [\varepsilon_{i,j,lb}, \varepsilon_{i,j,ub}]$ with

$$\varepsilon_{i,j,lb} = \min_{\mathbf{x},\mathbf{u},t_f} J_{S_i}, \quad \varepsilon_{i,j,ub} = J_{S_i}\left(\arg\min_{\mathbf{x},\mathbf{u},t_f} J_{S_j}\right). \tag{14}$$

for $i \neq j$. The bounds $\varepsilon_{i,0}$ and $\varepsilon_{0,j}$ for J_0 are defined analogously. To obtain the bounds, each cost is minimized in single-cost optimizations before solving the ε-constrained problems. By varying the bounds, all Pareto optimal solutions can be calculated, also if the frontier is non-convex [12].

3.3 Method of weighted metrics

In the method of weighted metrics, the distance to a reference vector is minimized:

$$\min_{\mathbf{x},\mathbf{u},t_f} \left(w_0 c_{m,0} \left(J_0 - J_0^*\right)^q + \sum_{i=1}^{n_J} w_i c_{m,i} \left(J_{S_i} - J_{S_i}^*\right)^q \right)^{\frac{1}{q}}$$

with $1 \leq q < \infty$ and J_0^* and $J_{S_i}^*$ commonly being the minimum of the according individual cost function. The minimization of the distance to the minimum can be seen as a kind of soft constraint, contrary to the hard constraint in the ε-constraint method in Section 3.2. The method can only represent all Pareto optimal solutions, if the problem is convex [12]. Similar to the weighted sum method description, each term is weighted with a scaling factor $c_{m,i}$ to scale the costs to a similar order of magnitude.

3.4 Weighted Tchebycheff method

A special case of the weighted metrics method for $q = \infty$ is the Tchebycheff formulation:

$$\min_{\mathbf{x},\mathbf{u},t_f} \max \left[w_0 c_{T,0} \left| J_0 - J_0^* \right|, w_1 c_{T,1} \left| J_{S_1} - J_{S_1}^* \right|, \ldots, w_{n_J} c_{T,n_J} \left| J_{S_{n_J}} - J_{S_{n_J}}^* \right| \right]. \tag{15}$$

Contrary to the weighted metrics method, only the maximum cost function is minimized. The method can represent any Pareto optimal point for a utopian reference vector, which is strictly smaller than the optimal vector $\left[J_0^*, J_{S_1}^*, \ldots, J_{S_{n_J}}^* \right]$ consisting of the minima of each individual cost as stated in [12]. Similar to the weighted sum method description, each term is weighted with a scaling factor $c_{T,i}$ to scale the costs to a similar order of magnitude.

It is to be noted that absolute values are difficult to handle in gradient-based optimization due to non-differentiability. However, the absolute values can be omitted since the minima J_0^* and $J_{S_i}^*$ are known. Furthermore, the maximum function is not differentiable. To handle this, a parameter $p_{max} \geq 0$ is introduced fulfilling

$$\begin{aligned} w_0 c_{T,0} \left(J_0 - J_0^* \right) &\leq p_{max}, \\ w_i c_{T,i} \left(J_{S_i} - J_{S_i}^* \right) &\leq p_{max}, \quad i = 1, \ldots, n_J. \end{aligned}$$

Then, the minimization (15) can equivalently be formulated by

$$\min_{\mathbf{x},\mathbf{u},t_f} p_{max}.$$

4 Application to robust UAV trajectory optimization

4.1 Problem statement

When planning missions for UAVs, it is of high interest to minimize operational costs while increasing robustness. The scenario studied in this paper is a climb in minimum time under consideration of uncertainties in the aerodynamic model adapted from [1]. To find a satisfactory trade-off between costs and robustness, an approximation of a Pareto front is calculated with the scalarization methods in Section 3. Specifically, positional sensitivities are minimized with an open-loop and a closed-loop model to assess the robustness performances. Therefore, a fixed-wing UAV is modeled with the dynamic equations as presented in [8] and [1]. The states x, y, h describe the positional coordinates. The course angle is denoted by χ, the flight path angle by γ and the velocity by V. Furthermore, m is the mass of the vehicle and g is the gravitational

acceleration. The dynamics are given as follows:

$$\begin{aligned}
\dot{x}(t) &= V(t)\cos\chi(t)\cos\gamma(t)\\
\dot{y}(t) &= V(t)\sin\chi(t)\cos\gamma(t)\\
\dot{h}(t) &= V(t)\sin\gamma(t)\\
\dot{\chi}(t) &= \frac{L(t)\sin\mu(t)}{mV(t)\cos\gamma(t)}\\
\dot{\gamma}(t) &= \frac{L(t)\cos\mu(t) - mg\cos\gamma(t)}{mV(t)}\\
\dot{V}(t) &= \frac{T(t) - D(t)}{m} - g\sin\gamma(t),
\end{aligned}$$

The thrust, lift and drag are given by

$$\begin{aligned}
T(t) &= \delta_T(t) T_{max}\\
L(t) &= \frac{1}{2}\rho V(t)^2 A C_L(t)\\
D(t) &= \frac{1}{2}\rho V(t)^2 A \left(C_{D_0} + k C_L(t)^2\right)
\end{aligned}$$

with T_{max} being the maximum thrust of the vehicle, ρ the air density, A the reference area, C_{D_0} the zero-lift drag coefficient and k the induced drag factor. The controls are given by the lift coefficient C_L, the bank angle μ and the thrust lever position δ_T. The model parameter values are given in Table 1.

Parameter	Unit	Value
m	kg	6
g	m/s	9.81
ρ	kg/m^3	1.225
T_{max}	N	70.632
A	m^2	0.7
C_{D_0}	-	0.015
k	-	0.02

Table 1: Model parameter values.

The task of the UAV is a climb in minimum time with the initial and final boundary conditions, path, and rate constraints as given in Tables 2 and 3. Furthermore, for a well-posed problem, a limitation for the flight time of maximally 20 s is set.

The uncertainty is assumed to be in the aerodynamic zero-lift drag coefficient C_{D_0} with a deviation up to 30 %. To reduce collision risk, a robust position for sufficient separation may be important for specific scenarios. Therefore, the sensitivities of the x-position and the altitude with respect to C_{D_0} defined by $S_x \coloneqq \frac{\partial x}{\partial C_{D_0}}$ and $S_h \coloneqq \frac{\partial h}{\partial C_{D_0}}$ are minimized as well. Then, the cost functions are given by

$$J_0 = t_f, \quad J_{S_1} = \int_{t_0}^{t_f} S_x(t)^2 \, dt, \quad J_{S_2} = \int_{t_0}^{t_f} S_h(t)^2 \, dt.$$

	Symbol	Unit	Lower Bound	Upper Bound	Initial Value	Final Value
States	x	m	0	∞	0	-
	y	m	0	∞	0	-
	h	m	0	∞	30	100
	χ	deg	-60	60	0	0
	γ	deg	-30	30	0	0
	V	m/s	0	20	17	17

Table 2: State limits and initial boundary conditions.

	Symbol	Unit	Lower Bound	Upper Bound
Controls	C_L	-	0	1
	μ	deg	-30	30
	δ_T	-	0	1
	$\mathbf{K}$	-	-0.5	0.5
Control Rates	$\dot{C}_L,\ \hat{\dot{C}}_L(\cdot, \mathbf{p}_{lb}),\ \hat{\dot{C}}_L(\cdot, \mathbf{p}_{ub})$	1/s	-0.1	0.1
	$\dot{\mu},\ \hat{\dot{\mu}}(\cdot, \mathbf{p}_{lb}),\ \hat{\dot{\mu}}(\cdot, \mathbf{p}_{ub})$	deg/s	-30	30
	$\dot{\delta}_T,\ \hat{\dot{\delta}}_T(\cdot, \mathbf{p}_{lb}),\ \hat{\dot{\delta}}_T(\cdot, \mathbf{p}_{ub})$	1/s	-0.1	0.1

Table 3: Control and rate limits.

To minimize the costs, the scalarization techniques presented in Section 3 are implemented. For the weighted methods, 11 equidistant weights for each $w_0, w_1, w_2 \in [0, 1]$ are perturbed fulfilling $\sum_{i=0}^{2} w_i = 1$ to cover different combinations of weighting triplets. Due to the different orders of magnitude between the cost functions in the open-loop case, each weighted cost term is scaled by a factor $c_{(s,m,T),i}$ to improve the balance between the cost terms. The index refers to the weighted sum (s), weighted metrics (m), and the Tchebycheff method (T). The values are given in Table 4. Since in the closed-loop case, the cost values are in a similar order of magnitude in the region of interest, the scaling factors are set to 1.

In the weighted metric sum method, the exponent $q = 2$ is chosen, i.e., the Euclidean norm. For the ε-constraint method, the weighted metric sum, and the weighted Tchebycheff method, a range for the bounds and reference values are required. These are determined by solving each single-objective optimization problem according to the equations in (14). For the closed-loop case, the upper bounds are determined after a first run of multi-objective optimizations and after observing that the sensitivity costs vary in the order of magnitude. This observation led to the selection of smaller bound intervals to map the relevant region of solutions. Therefore, 11 upper bounds $\varepsilon_{i,j}$ are equidistantly chosen within the intervals given in Table 4. The optimal control problems are solved with the framework FALCON.m [14], which is based on direct optimal control using trapezoidal collocation and the optimization solver IPOPT [2].

4.2 Numerical results

The optimal cost function values using the scalarization techniques from Section 3 for the open-loop and closed-loop case are depicted in Fig. 1 and Fig. 2, respectively. The first observation is that the approximation of both Pareto fronts are likely to be convex.

In the open-loop solutions, the scalarization techniques deliver similar approximations of a

	Open-loop	Closed-loop
J_0^*	9.0539 s	9.0524 s
$c_{s,0}$	1	1
$c_{m,0}$	1	1
$c_{T,0}$	1	1
$\varepsilon_{0,1}$	$[9.0539, 12.4507]$ s	$[9.0524, 15]$ s
$\varepsilon_{0,2}$	$[9.0539, 10.6350]$ s	$[9.0524, 15]$ s
$J_{S_1}^*$	9.1757×10^3	0.0146
$c_{s,1}$	$1/9000$	1
$c_{m,1}$	10^{-10}	1
$c_{T,1}$	$1/9000$	1
$\varepsilon_{1,0}$	$[9.1757 \times 10^3, 3.9171 \times 10^5]$	$[0.0146, 20]$
$\varepsilon_{1,2}$	$[9.1757 \times 10^3, 4.2593 \times 10^4]$	$[0.0146, 20]$
$J_{S_2}^*$	6.3733×10^4	1.3177×10^{-7}
$c_{s,2}$	10^{-5}	1
$c_{m,2}$	10^{-10}	1
$c_{T,2}$	10^{-5}	1
$\varepsilon_{2,0}$	$[6.3733 \times 10^4, 6.3653 \times 10^5]$	$[1.3177 \times 10^{-7}, 20]$
$\varepsilon_{2,1}$	$[6.3733 \times 10^4, 3.6027 \times 10^5]$	$[1.3177 \times 10^{-7}, 20]$

Table 4: Parameters for scalarized multi-objective optimization problems.

Pareto front with slightly different distributions of solutions on the frontier. The results show that a relevant region of an acceptable trade-off may be between 10 s and 11 s, where the deviations in the x-position and altitude can be reduced to be below 1 m and 2 m, respectively. With the weighted methods, the solutions are mainly concentrated in an area between 10 s and 12 s, including the region of interest. In contrast, the ε-constraint technique delivers points over the whole frontier, also in a surrounding of extreme cases, i.e., close to the minimum of the single costs.

In the closed-loop solutions, the cost function values have varying orders of magnitude from 1 to 10^5. Therefore, the selection of bounds for the ε-constraint method is based on a relevant region with low sensitivities to be considered by a decision maker under the assumption that a decision maker would exclude solutions with high sensitivities. Approximate Pareto optimal solutions in this region are depicted in Fig. 2. In the ε-constraint method, the solutions are more evenly distributed over the approximate frontier. The weighted methods deliver solutions concentrated in the center of the region. Exemplary state trajectories and nominal controls with an acceptable trade-off resulting from the ε-constraint method are depicted in Fig. 3. The reduction of sensitivities, i.e., the increase in robustness, is significant compared to the open-loop solutions. Trajectories with near-optimal flight time and reduced positional deviations below 2 cm can be obtained using the actual parameter value. Employing perturbed parameter values assuming that a drag estimator can reduce the estimation uncertainty to 5 %, the positional deviations are below 15 cm, i.e., the predicted feedback leads to good robustness performance when considering estimation errors in parameter values. The trajectory structures of potentially Pareto optimal solutions in Fig. 3 indicate that robust solutions may reduce the overall velocity during flight, increasing flight time, similar to the studies in [1]. It is to be noted that the results are specific to the selected gain bounds. The fact that the closed-loop solutions fully exploit

these bounds, i.e., the bound constraints are active for some time points, may indicate that robustness could be improved by increasing the gain bounds, provided that feasible solutions exist.

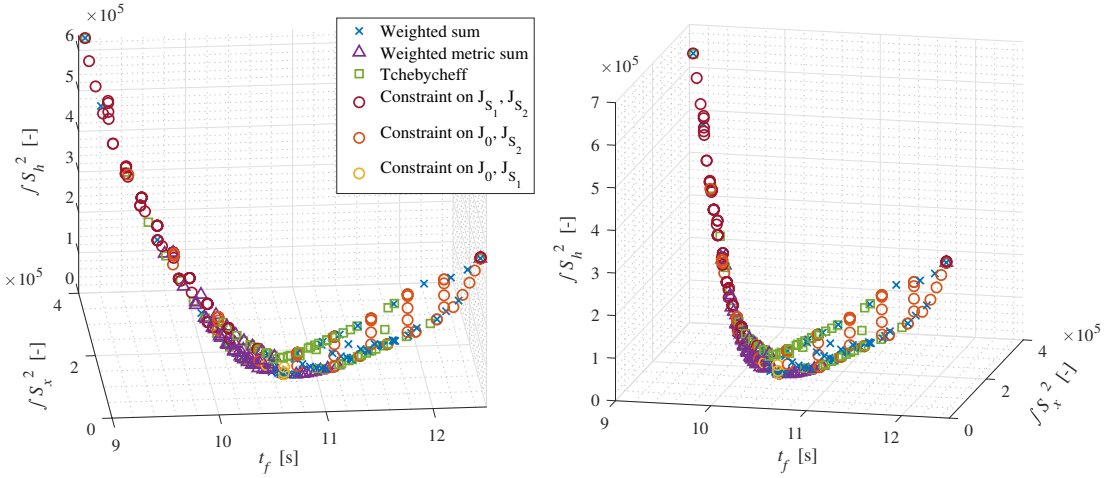

Figure 1: Approximation of Pareto front for open-loop problem formulation from different perspectives.

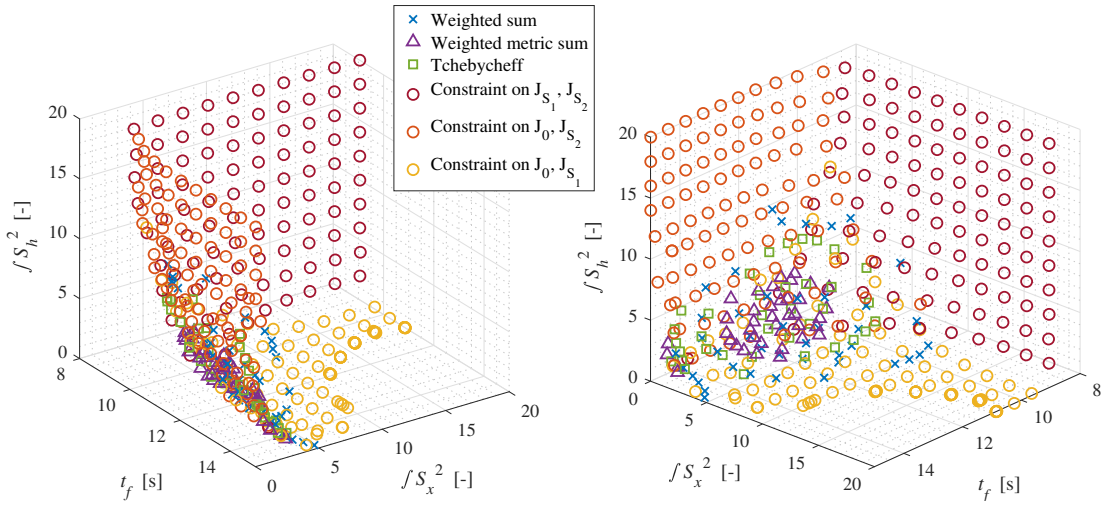

Figure 2: Approximation of Pareto front for closed-loop problem formulation from different perspectives.

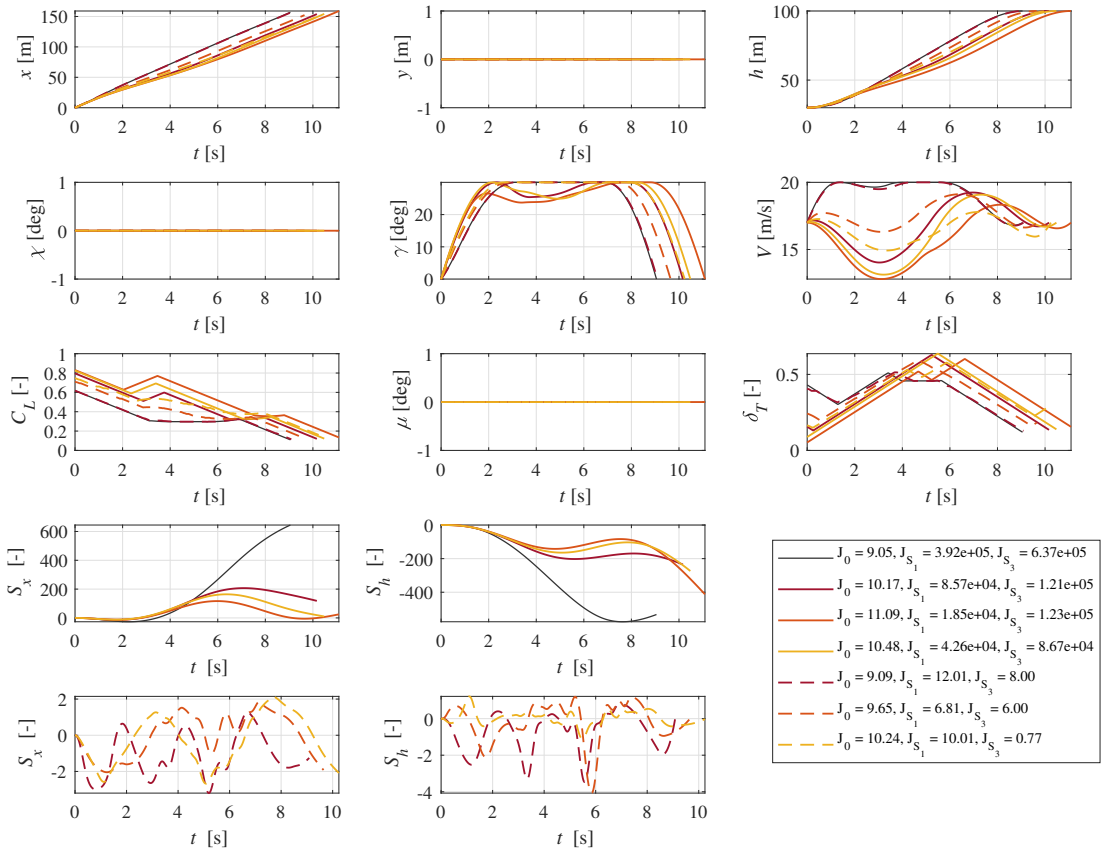

Figure 3: Selected robust trajectories with an acceptable trade-off resulting from ε-constraint method in open-loop (solid) and closed-loop (dashed) modeling compared to the optimal nominal open-loop trajectories (black).

5 Conclusion and outlook

This study analyzes multi-objective solutions to map the trade-off between optimality of operational costs and robustness in UAV trajectory optimization, considering open-loop and closed-loop modeling approaches. By adapting the weights and bounds to the different orders of magnitude of costs, the weighting techniques and the ε-constraint technique deliver relevant sets of approximate Pareto optimal solutions. The analysis serves as a basis for a decision maker to choose a solution with an acceptable trade-off and for evaluating the performance of an open-loop and a closed-loop sensitivity minimization approach for further improvements. It is observed that the closed-loop solutions depend on the user-defined gain bounds and further research can be directed to investigate suitable gain bounds in order to enhance a robust closed-loop strategy. Furthermore, the solutions may be improved by investigating globalization techniques for better approximation of Pareto optima and by analyzing Pareto optimality.

6 Acknowledgments

The authors would like to thank Prof. Joseph Z. Ben-Asher and Felix Schweighofer for valuable comments and discussions.

References

[1] T. Akman, J. Z. Ben-Asher, and F. Holzapfel. Approximation of closed-loop sensitivities in robust trajectory optimization under parametric uncertainty. *Aerospace*, 11(8):640, 2024.

[2] L. T. Biegler and V. M. Zavala. Large-scale nonlinear programming using IPOPT: An integrating framework for enterprise-wide dynamic optimization. *Computers & Chemical Engineering*, 33(3): 575–582, 2009.

[3] M. Bittner, B. Fleischmann, M. Richter, and F. Holzapfel. Optimization of ATM scenarios considering overall and single costs. In *6th International Conference on Research in Air Transportation*, 2014. URL https://www.icrat.org/previous-conferences/6th-international-conference/papers/.

[4] R. Caballero, L. Rey, F. Ruiz, and M. González. An algorithmic package for the resolution and analysis of convex multiple objective problems. In G. Fandel and T. Gal, editors, *Multiple Criteria Decision Making*, volume 448 of *Lecture Notes in Economics and Mathematical Systems*, pages 275–284. Springer, Berlin and Heidelberg, 1997.

[5] M. Gerdts. *Optimal Control of ODEs and DAEs*. De Gruyter, Berlin and Boston, 2011.

[6] T. Han, C. Xu, R. Loxton, and L. Xie. Bi-objective optimization for robust RGB-D visual odometry. In *The 27th Chinese Control and Decision Conference (2015 CCDC)*, pages 1837–1844. IEEE, 2015. doi:10.1109/CCDC.2015.7162218.

[7] C. Hillermeier. *Nonlinear Multiobjective Optimization: A Generalized Homotopy Approach*, volume 135 of *International Series of Numerical Mathematics*. Birkhäuser Basel, 2001.

[8] H. Hong, P. Piprek, R. J. M. Afonso, and F. Holzapfel. Trigonometric series-based smooth flight trajectory generation. *IEEE Transactions on Aerospace and Electronic Systems*, 57(1):721–728, 2021.

[9] C. Y. Kaya and H. Maurer. Optimization over the pareto front of nonconvex multi-objective optimal control problems. *Computational Optimization and Applications*, 86(3):1247–1274, 2023.

[10] R. Loxton, K. L. Teo, and V. Rehbock. Robust suboptimal control of nonlinear systems. *Applied Mathematics and Computation*, 217(14):6566–6576, 2011.

[11] R. T. Marler and J. S. Arora. Survey of multi-objective optimization methods for engineering. *Structural and Multidisciplinary Optimization*, 26(6):369–395, 2004.

[12] K. Miettinen. Some methods for nonlinear multi-objective optimization. In E. Zitzler, L. Thiele, K. Deb, C. A. Coello Coello, and D. Corne, editors, *Evolutionary Multi-Criterion Optimization*, volume 1993 of *Lecture Notes in Computer Science*, pages 1–20. Springer, Berlin and Heidelberg, 2001.

[13] P. Piprek and F. Holzapfel. Bi-level trajectory optimization by stochastic collocation for uncertainty interval calculation. In *31st Congress of the International Council of the Aeronautical Sciences (ICAS 2018)*, pages 2928–2937, 2018. URL https://www.icas.org/ICAS_ARCHIVE/ICAS2018/data/preview/ICAS2018_0221.htm.

[14] M. Rieck, M. Bittner, B. Grüter, J. Diepolder, P. Piprek, C. Göttlicher, F. Schwaiger, B. Hosseini, F. Schweighofer, T. Akman, and F. Holzapfel. FALCON.m user guide: version 1.30, 2023. URL http://www.falcon-m.com.

[15] E. S. Rudnick-Cohen, S. Azarm, and J. Herrmann. Multi-objective design and path planning optimization of unmanned aerial vehicles (UAVs). In *16th AIAA/ISSMO Multidisciplinary Analysis and Optimization Conference*, pages 12–18, Reston, Virginia, 2015. American Institute of Aeronautics and Astronautics. doi:10.2514/6.2015-2322.

[16] K. Seywald and H. Seywald. Desensitized optimal control. In *AIAA Scitech 2019 Forum*, 2019. doi:10.2514/6.2019-0651.

[17] G. Sun, J. Li, Y. Liu, S. Liang, and H. Kang. Time and energy minimization communications based on collaborative beamforming for UAV networks: A multi-objective optimization method. *IEEE Journal on Selected Areas in Communications*, 39(11):3555–3572, 2021.

[18] M. Wang, S. O. D. Luiz, S. Zhang, and A. M. N. Lima. Desensitized optimal control of electric aircraft subject to electrical–thermal constraints. *IEEE Transactions on Transportation Electrification*, 8(4):4190–4204, 2022.